Accepted Manuscript

The design and SAR of a novel series of 2-aminopyridine based LRRK2 inhibitors

Garrick P. Smith, Lassina Badolo, Victoria Chell, I-Jen Chen, Kenneth Vielsted Christensen, Laurent David, Justus Alfred Daechsel, Morten Hentzer, Martin Christian Herzig, Gitte Kobberøe Mikkelsen, Stephen P. Watson, Douglas S. Williamson

Please cite this article as: Smith, G.P., Badolo, L., Chell, V., Chen, I-J., Christensen, K.V., David, L., Daechsel, J.A., Hentzer, M., Christian Herzig, M., Mikkelsen, G.K., Watson, S.P., Williamson, D.S., The design and SAR of a novel series of 2-aminopyridine based LRRK2 inhibitors, *Bioorganic & Medicinal Chemistry Letters* (2017), doi: http://dx.doi.org/10.1016/j.bmcl.2017.07.072

Graphical Abstract

To create your abstract, type over the instructions in the template box below.
Fonts or abstract dimensions should not be changed or altered.

The design and SAR of a novel series of 2-aminopyridine based LRRK2 inhibitors

Garrick P. Smith,* Lassina Badolo, Victoria Chell, I-Jen Chen, Kenneth Vielsted Christensen, Laurent David, Justus Alfred Daechsel, Morten Hentzer, Martin Christian Herzig, Gitte Kobberøe Mikkelsen, Stephen P. Watson, and Douglas S. Williamson
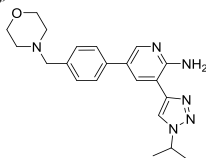
45 - LRRK2 WT IC_{50}=300 nM, cKi=7 nM

Bioorganic & Medicinal Chemistry Letters

journal homepage: www.elsevier.com

The design and SAR of a novel series of 2-aminopyridine based LRRK2 inhibitors

Garrick P. Smith*,[a] Lassina Badolo,[a] Victoria Chell,[b] I-Jen Chen,[b] Kenneth Vielsted Christensen,[a] Laurent David,[a] Justus Alfred Daechsel,[a] Morten Hentzer,[a] Martin Christian Herzig,[a] Gitte Kobberøe Mikkelsen,[a] Stephen P. Watson[a] and Douglas S. Williamson[b]

[a]H. Lundbeck A/S, Ottiliavej 9, 2500 Valby, Denmark

[b]Vernalis (R&D) Ltd., Granta Park, Great Abington, Cambridge, CB21 6GB, United Kingdom

ARTICLE INFO

ABSTRACT

Leucine-rich repeat kinase 2 (LRRK2) has attracted considerable interest as a therapeutic target for the treatment of Parkinson's disease. Compounds derived from a 2-aminopyridine screening hit were optimised using a LRRK2 homology model based on mixed lineage kinase 1 (MLK1), such that a 2-aminopyridine-based lead molecule **45**, with *in vivo* activity, was identified.

Leucine-rich repeat kinase 2 (LRRK2) has attracted considerable interest as a therapeutic target for Parkinson's disease (PD)[1-5], since autosomal-dominant missense mutations in LRRK2 have been associated with an increased risk of this neurological disorder. The pathogenic LRRK2 variant G2019S has elevated kinase activity, and so potent, selective and brain-penetrant inhibitors of LRRK2, which reduce its kinase activity, are needed to validate LRRK2 inhibition as a means of therapeutic intervention for PD. Compounds such as LRRK2-IN-1 (**1**)[6], GNE-7915 (**2a**)[7], PF-06447475 (**2b**)[8] and MLi-2 (**2c**)[9] have been used to elucidate the biology of LRRK2 in preclinical models.
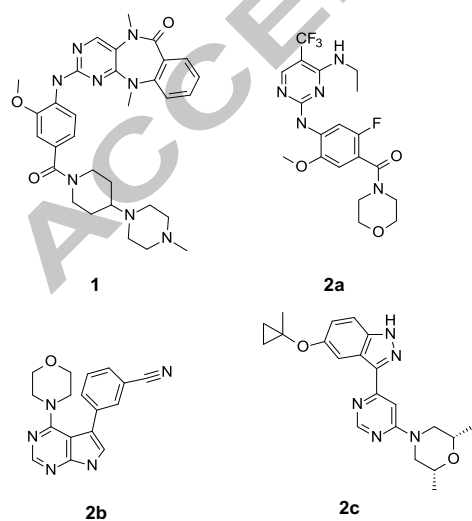
We initiated a medicinal chemistry effort to identify novel LRRK2 inhibitors with potential for lead optimization. The 2-aminopyridine **3a** was identified as a hit from our in-house screening collection. 2-Aminopyridines are well known to possess kinase inhibitory activity: for example, Crizotinib **3b** is a *c*-Met/ALK inhibitor approved for the treatment of non-small cell lung carcinoma (NSCLC) in the US[10].
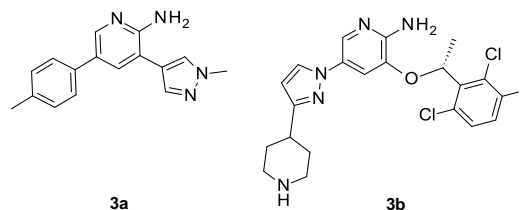
In order to guide the optimization of **3a**, a homology model was constructed, based on mixed lineage kinase 1 (MLK1) and refined using known LRRK2 binders. The binding model of compound **3a** was modelled using Glide[11] and shown in Figure 1A. The hinge binding scaffold of compound **3a** is suggested to be the 2-aminopyridine group, which forms two hydrogen bonds to the backbone atoms of Glu1948 and Ala1950 in the hinge of the ATP binding site of the LRRK2 kinase domain. The methyl pyrazole group positions its methyl substituent close to Ala2016, a residue important for selectivity as this position varies across kinases. The phenyl at the 5-position of the pyridine ring extends along the hinge region towards the solvent. Compound **3a** demonstrated good apparent permeability in the MDCK cell line, indicating potential for central nervous system (CNS) penetration, as detailed in Table 1. This was accompanied by high *in vitro* intrinsic clearance, observed in both human and rat

liver microsomes. A low molecular weight of 264, a CNS multiparameter optimization (MPO) score[12] of 5.4, and a ligand lipophilicity effiency[13] (LLE) towards LRRK2 G2019S of 3.71, however, encouraged us to pursue **3a**. The aim of the initial hit exploration was to improve the *in vitro* potency and the pharmacokinetic profile sufficiently for identifying a lead molecule with *in vivo* potency. Herein, we report the SAR around this 2-aminopyridine scaffold, where the 3-pyrazolyl and 5-tolyl substituents of **3a** are modulated.
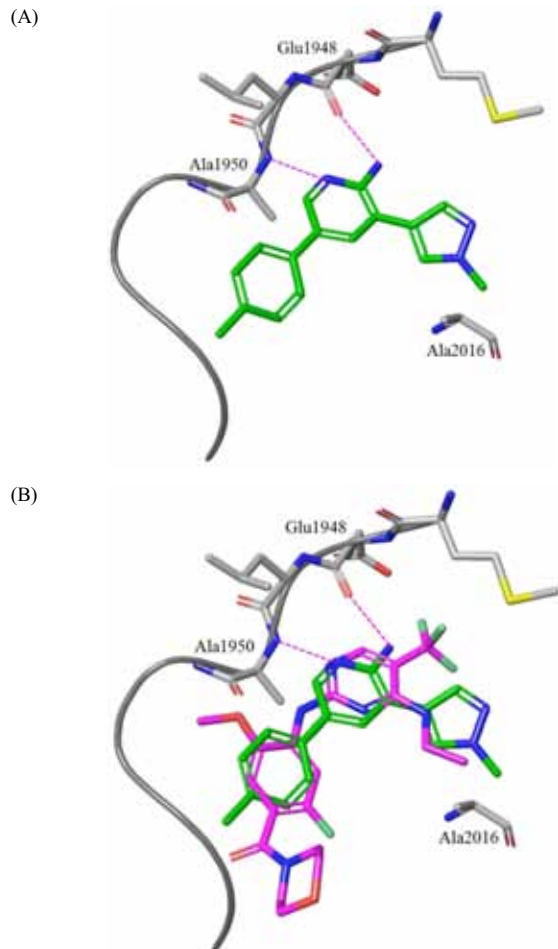
(A)

(B)

Figure 1. (A) Binding mode of **3a** (green) in LRRK2 homology model. The hinge region of LRRK2 ATP binding site is shown in grey tube. Two hydrogen bonds formed between **3a** and LRRK2 are highlighted in broken magenta lines. (B) Binding mode of **2a** (GNE-7915, magenta) in same LRRK2 homology model and superposed with **3a** (green). Hydrogen bonds between the hinge binding motif and LRRK2 are highlighted in broken magenta lines.

Table 1. *In vitro* profile of 2-aminopyridine hit **3a**.

|	
LRRK2 G2019S IC$_{50}$	6.7 µM
(LRRK2 G2019S calc. K_i	0.46 µM, LE 0.43)
LRRK2 WT IC$_{50}$	16 µM
(LRRK2 WT calc. K_i	0.51 µM, LE 0.44)
Human Liver Microsomes	6 L/kg/h
Rat Liver Microsomes	17 L/kg/h
MDCK Papp	16.9 x 10^{-6} cm/s
MDCK (B-A/A-B) Ratio	0.55

Compound **3a** and analogues were prepared according to chemistries outlined in Schemes 1–6. Compounds where the 3-pyrazole was replaced whilst the 5-tolyl substituent was kept constant are shown in Scheme 1, and this approach was used for the preparation of compounds **3a** and **28**–**31.** The tolyl group was introduced by Suzuki coupling between 2-amino-5-bromopyridine **4** and 4-methylphenyl boronic acid to give **5**. Subsequent bromination gave **6**, which allowed the introduction of a heteroaryl group *via* a second Suzuki or Stille coupling to give **7**. Compounds **36**, **37** and **42** were prepared as shown in Scheme 2. 3-Bromo-2-aminopyridine **8** could be employed to introduce the 3-heteroaryl ring via Suzuki coupling to give **9**, followed by bromination to give **10**, and then a second coupling to give **11**. Additionally, 3-heteroaryl rings could be constructed, as shown in Schemes 3, 4, 5 and 6.

Scheme 1
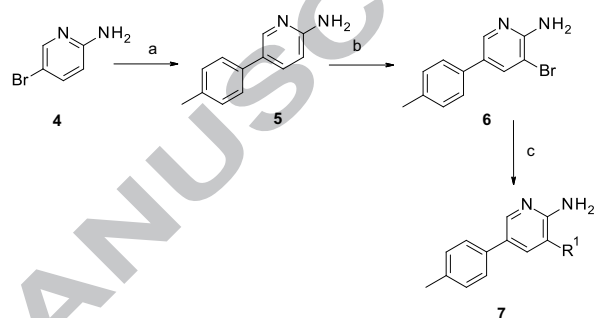
Reagents and conditions: (a) 4-Methylphenylboronic acid, Pd(PPh$_3$)$_4$, 1,4-dioxane, H$_2$O, 100 ºC, 3h, 88%; (b) *N*-bromosuccinimide, acetonitrile, 30 min, 64%; (c) R^{1}B(OH)$_2$ or R^{1}SnBu$_3$, Pd(Ph$_3$P)$_4$, Cs$_2$CO$_3$, 1,4-dioxane.

Scheme 2
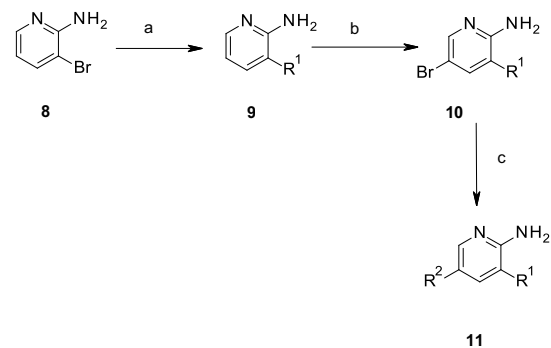
Reagents and conditions: (a) R^{1}B(OH)$_2$ or R^{1}B(C$_2$O$_2$(CH$_3$)$_4$), Cs$_2$CO$_3$, Pd(PPh$_3$)$_4$, 1,4-dioxane, H$_2$O; (b) *N*-bromosuccinimide, KOAc, DMF, 80 ºC, 60 min; (c) R^{2}B(OH)$_2$, Pd(Ph$_3$P)$_4$Cs$_2$CO$_3$, 1,4-dioxane, H$_2$O.

Triazole derivative **16** was prepared as shown in Scheme 3. 5-Bromo-3-aminopyridine **12** was converted to ethyl carbamate **13**. Introduction of the tolyl group using Suzuki methodology gave **14**. Hydrolysis of the ethyl carbamate and subsequent conversion of the aniline to the nitrofluoropyridine **15** allowed S$_N$Ar displacement using 4-methyl-1*H*-(1,2,3)-triazole and subsequent reduction of the nitro group to obtain triazole derivative **16.**

Scheme 3
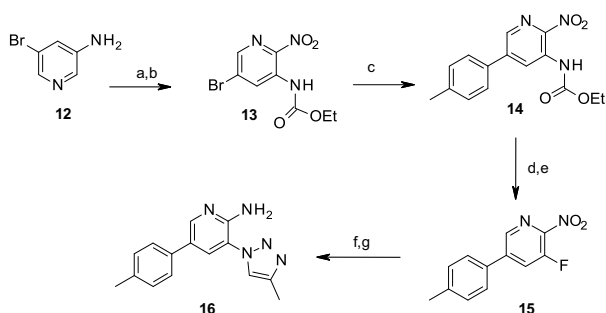

Reagents and conditions: (a) ClCO₂Et, 0°C, 30 min; (b) H₂SO₄, HNO₃, 0°C to r.t., 16 h; (c) 4-tolylboronic acid, Pd(PPh₃)₄, Cs₂CO₃, 1,4-dioxane–water (7:3), 90°C, 16 h; (d) KOH, H₂O, 100 °C, 6 h; (e) HBF₄, NaNO₂, 0 °C to r.t., 4h; (f) 4-methyl-1*H*-(1,2,3)-triazole, K₂CO₃, DMF; (g) H₂, Pd/C, H₂, EtOH.

The 2-methyloxazole derivative **18** was prepared, as shown in Scheme 4. Introduction of an acetyl group by reaction of **6** with (1-ethoxyvinyl)tributyltin under palladium catalysis gave **17**. This then allowed formation of the 2-methyloxazole derivative **18**, using dimethylacetamide dimethyl acetal and hydroxylamine.

Scheme 4
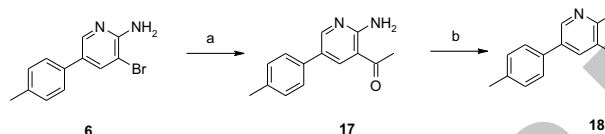
Reagents and conditions: (a) tris-*n*-butyl(1-ethoxyvinyl)stannane, Pd(PPh₃)₂Cl₂, 1,4-dioxane, 100 °C, 18 h; (b) (i) *N,N*-dimethylacetamide dimethylacetal, 100 °C, 18 h; (ii) NH₂OH.HCl, EtOH, 90 °C, 24 h.

1,3,4-Oxadiazole derivatives **32–35**, **38–40** and 1,2,4-oxadiazole **24** were prepared as shown in Scheme 5. 2-Amino-nicotinic acid **19** was brominated to give **20**. This was converted to the 1,3,4-oxdiazole **21** using the appropriately-substituted acetyl hydrazine, or to the 1,2,4 oxadiazole **23** using *N*-hydroxyacetamidine. Subsequent Suzuki coupling of **21** or **23** with the desired aryl boronic acid afforded 1,3,4-oxadiazoles of the general structure **22**. In the case of compound **35**, coupling of 5-*N*-methylindolylboronic acid and a final reductive step using triethysilane was employed (step e). Suzuki coupling of 5-indolylboronic acid yielded 1,2,4-oxadiazole **24.**

Scheme 5
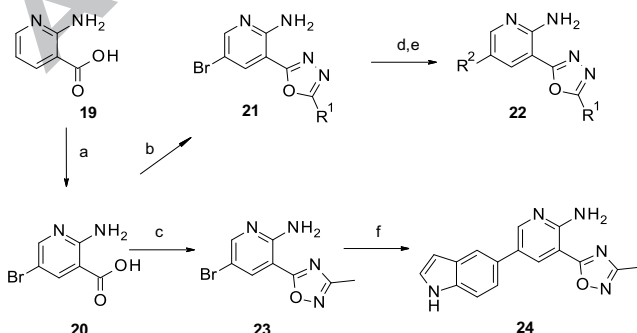
Reagents and conditions: (a) Br₂, AcOH, r.t., 18 h; (b) R¹CONHNH₂, POCl₃, 100 °C, (c) *N*-hydroxyacetamidine, TBTU, HOBt, DMF, r.t. 12 h, 78%. , (d) R²B(OH)₂, Pd(PPh₃)₄, K₂CO₃, dioxane, water, 100 °C, 18 h (e) cpd **35** only Et₃SiH, TFA, 0 °C, 2 h, 50% ;(f) 5-Indolylboronic acid, Pd(PPh₃)₄, Cs₂CO₃, dioxane, water, 100 °C, 6 h, 3%

Triazole derivatives **41** and **43–45** were prepared as shown in Scheme 6. Cycloaddition of the alkyne **25** with isopropyl azide gave triazole **26**. Coupling under Suzuki conditions with the appropriate boronic acid gave the final product **27**.

Scheme 6
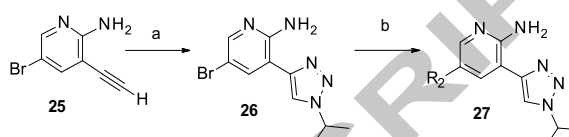
Reagents and conditions: (a) Isopropyl azide, CuI, *t*-BuOH/H₂O, 16 h, 65%; (b) R²-boronate pinacol ester, Pd(PPh₃)₄, Cs₂CO₃, ethylene glycol dimethyl ether/H₂O, 140 °C, microwave, 6 h.

Initial structural exploration of **3a** by variation of R¹ with a range of substituted 5-membered nitrogen-containing heterocycles is described in Table 2. Removal of the methyl substituent, as in **28**, or the addition of the larger ethyl (**30**) had modest effects on activity. Addition of an extra methyl in the 1,5-dimethylpyrazole **29** abolished activity. The 4-(1-methylimidazole) **31** was weakly active, whilst the 1,3-oxazole **18** and triazole **16** showed comparable potencies to **3a**. An improvement in activity was observed with the 2-cyclopropyl-1,3,4- oxadiazole substitution, as seen with **32**.

Amongst all groups tried at R¹, oxadiazole **32** showed the greatest improvement in LRRK2 inhibition, compared to starting point **3a**. To understand the reasons for this, compound **32** was modelled in the same LRRK2 homology model as described earlier. In Figure 2, the binding mode of **32** was predicted to be very similar to compound **3a** regarding hinge binding motif. A difference in coplanarity between compounds **32** and **3a** was observed. The dihedral angle (φ) between 2-aminopyridine and oxadiazole was calculated to be 2.9 degrees (Figure 3), as opposed to 21 degrees for compound **3a**. The higher φ value required for compound **3a** is to avoid steric clashes of protons coming from the amino group and the 3'-position of the pyrazole. On the contrary, a much lower φ was predicted for the oxadiazole because one of the oxadiazole nitrogens is now able to intramolecularly hydrogen bond to the amino NH. The coplanarity is further enhanced by the presence of oxygen in the 5-membered aryl ring not incurring further twist with respect to the pyridine ring. Such coplanarity appears to be beneficial for LRRK2, possibly because of binding site complementarity. In addition, the cyclopropyl affords better contact with Ala2016, which was not possible with compound **3a**.

Table 2. Effect of pyrazole ring R^1 modifications on LRRK2 inhibition.
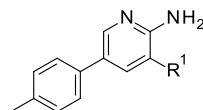
Compound	R^1	LRRK2 G2019S IC_{50} / cK_i (μM)	LRRK2 WT IC_{50}/ cK_i (μM)
GNE7915	-	0.046/0.0011	0.097/0.0011
3a		6.7/0.46	16/0.51
16		9.1/0.63	70% inhib @ 30 μM /n.d.
28		13/0.76	72%inhib @ 66.7μM/1.0
18		11/0.63	24/0.72
29		62% inhib @ 200 μM/5.4	49% inhib @200 μM/4.7
30		12/0.7	12/0.37
31		57/3.3	60% inhib @200 μM/3.5
32		2.2/0.13	2.3/0.068
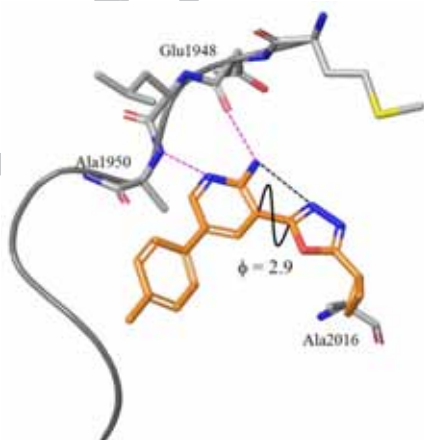
Figure 2. Binding mode of **32** (orange) in LRRK2 homology model. The hinge region of the LRRK2 ATP binding site is shown in grey tube. Two hydrogen bonds formed between **32** an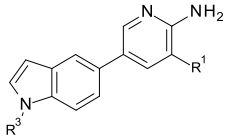d LRRK2 are highlighted in broken magenta lines. The cyclopropyl group of **32** is in close contact with Ala2016. The dihedral angle (φ) between the 2-amino and oxadiazole group is predicted to be 2.9 degrees. The potential intramolecular hydrogen bond between the amino and oxadiazole groups is shown as a broken black line.

The clear improvement in potency at the R^1 position with the 1-cyclopropyl-1,3,4-oxadiazole was followed up with a small variation of the 5- position as shown in Table 3. The 5-indole substituent **33** was moderately potent, whilst potency improvements were observed with the *N*-methylmorpholine derivative **34** and the *N*-methyl 5-indoline **35**.

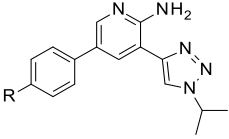**Table 3**. Effect of tolyl R^2 replacements on LRRK2 inhibition.
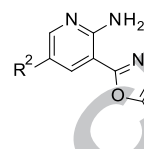
Compound	R^2	LRRK2 G2019S IC_{50}/ cK_i (μM)	LRRK2 WT IC_{50}/ cK_i (μM)
33		1.6/0.1	1.3/0.037
34		0.39/0.027	0.49/0.012
35		0.71/0.048	0.97/0.023

Re-examination of R^1 with the 5-indole group as R^2 was then undertaken, and the results are listed in Table 4. The 5-indole equivalent (**36**) of compound **3a** displayed similar potency, whilst the corresponding 3-pyrazole regioisomer **37** was much weaker. Compound **42**, with a methyl on the indole nitrogen, resulted in a modest improvement of potency compared to the desmethyl analogue **36.** The 1,2,4-oxadiazole **24** was inactive. This is likely caused by the methyl group being incompatible with the binding site, as a result of a possible intramolecular hydrogen bond between R^1 and the 2-amino group. The 1,3,4-oxadiazole derivatives **38**, **39** and **40** showed promising potency, of which the 2-isopropyl-1,3,4-oxadiazole derivative **39** was the most potent. The isopropyl substituent was the most potent on the 1,3,4-oxadiazole derivatives, and methylated indole also seems to give an improved potency. These optimal substituents were therefore combined in the triazole derivative **41**. This compound displayed improved potency compared to **36**.

Table 4. Effect of R^1 and R^3 substitution on LRRK2 inhibition.

Compound	R^1	R^3	LRRK2 G2019S IC$_{50}$/cK_i (μM)	LRRK2 WT IC$_{50}$/cK_i (μM)
36		H	13/ 0.8	75% inhib @ 200 μM/ n.d.
37		H	65% inhib @ 40 μM/ n.d.	48% @200 μM/ n.d.
38		H	3.6/0.25	n.d.
24		H	n.a./ n.d.	n.a./ n.d.
39		H	0.91/0.063	n.d.
40		H	2.9/0.17	77% inhib @22μM/0.19
41		Me	0.54/0.037	0.55/0.013
42		Me	5.8/0.48	64% inhib @ 30μM/n.d.

Based on proposed binding models of the 2-aminopyridine series (Figures 1 and 2), it was clear that the 4 position of the R^2 phenyl points to solvent, hence a good vector to use for improving physicochemical properties. Attempts to improve the physicochemical properties of this series of 2-aminopyridine based LRRK2 inhibitors by replacement of the indole with water solubilizing groups attached to the 4 position of the R^2 phenyl group are shown in Table 5. As can be seen, little difference was observed in LRRK2 inhibitory activity between compounds **43**, **44** and **45** suggesting there was space for incorporation of solubilizing groups in this position.

Table 5. Effect of morpholine substitution on LRRK2 inhibition.

Compound	R	LRRK2 G2019S IC$_{50}$/cK_i (μM)	LRRK2 WT IC$_{50}$/cK_i (μM)
43		0.28/0.020	0.34/0.08
44		0.34/0.023	0.60/0.014
45		0.16/0.011	0.30/0.007

Encouragingly, the most potent compound **45** (LRRK2 G2019S calc. K_i 11 nM) had an LE of 0.39, which compared favourably with that of the start point **3a** (LE 0.43, based on LRRK2 G2019S calc. K_i 460 nM). Compound **45** had an aqueous solubility measured to be 36 μg/mL at pH 7.4; an improvement compared to 11 μg/mL for compound **3a**. Compound **45** was profiled in more depth to ascertain its suitability for lead optimization. The compound was assessed in the human MDCK assay as having good permeability with no efflux liability. Intrinsic clearance was assessed to be low in human and moderate in rat liver microsomes (LM). These properties, together with a high MPO score of 5.70, LLE of 5.90 and acceptable molecular weight of 378.5, encouraged us to investigate this compound further.

Table 6. Key *in vitro* parameters for **45**.

LRRK2 G2019S IC$_{50}$	160 nM
(LRRK2 G2019S calc. K_i	11 nM, LE 0.39)
LRRK2 WT IC$_{50}$	300 nM
(LRRK2 WT calc. K_i	7 nM, LE 0.40)
Human Liver Microsomes	1.2 L/kg/h
Rat Liver Microsomes	9.4 L/kg/h
MDCK Papp	26.33 x 10^{-6} cm/s
MDCK Ratio (B-A)/(A-B)	0.68

Good CNS penetration was observed in mouse brain at a dose of 10 mg/kg po, with a total b/p ratio of 1.3 (K$_{p\,u,u}$=0.76) and a free brain concentration estimated to be 159 nM based on *in vitro* estimation of unbound brain fraction using equilibrium dialysis of brain homogenate and buffer. Cellular potency was estimated by monitoring inhibition of Ser935 phosphorylation in HEK293 cells transiently expressing LRRK2 WT or LRRK2 G2019S. The cell-based IC$_{50}$'s were measured to be 2100 and 920 nM, respectively.

Kinase selectivity of compound **45** was assessed in human peripheral blood mononuclear cells at 1 μM using the Kinativ^{TM} screening technology.[14] Good selectivity was demonstrated against 208 kinase sites with cross reactivity only being observed against ULK (40.8%) and MAP3K1 (83.3%). Activity against LRRK2 was moderate, with 48.5% inhibition observed.

A study of the *in vivo* pharmacodynamic effect of **45** on inhibition of LRRK2 Ser935 phosphorylation was undertaken. *In vivo* dosing of **45** at 50 mg/kg sc in mice showed 76% and 79% inhibition of Ser935 phosphorylation in brain and kidney respectively. Mean plasma and brain free concentrations of **45** were 1451 nM and 877 nM, respectively.

In summary, using a LRRK2 homology model based on MLK1, we have undertaken optimisation of a novel class of LRRK2 inhibitors in order to identify lead(s) such as compound **45,** which are sufficiently potent and brain penetrant to have *in vivo* activity and as such are useful for further exploration.

References and notes

[1]   Christensen, K. V.; Smith, G. P.; Williamson, D. S. Development of LRRK2 Inhibitors for the Treatment of Parkinson's Disease. In *Progress in Medicinal Chemistry*; Witty, D. R., Cox, B., Eds.; Elsevier, **2017**, *56*, 37–80.

[2]   Taymans, J.; Greggio, E. *Curr. Neuropharmacolog*. **2016**, *14, 214-22.*

[3]   Kethiri, R. R.; Bakthavatchalam, R. *Expert Opin . Ther. Patents* **2014**, *24*, 745–757.

[4]   Estrada, A. A.; Sweeney, Z. K. *J. Med. Chem.* **2015**, *58*, 6733–6746.

[5]   Zhu, H.; Chen, H.; Cho, W.; Estrada, A. A.; Sweeney, Z. K. *Med. Chem. Approaches to Pers. Med.* **2014**, 227–254.

[6]   Deng, X.; Dzamko, N.; Prescott, A.; Davies, P.; Liu, Q.; Yang, Q.; Lee, J.-D.; Patricelli, M. P.; Nomanbhoy, T. K.; Alessi, D. R.; Gray, N. S. *Nat. Chem. Biol.* **2011**, *7*, 203–5.

[7]   Estrada, A. A.; Liu, X.; Baker-Glenn, C.; Beresford, A.; Burdick, D. J.; Chambers, M.; Chan, B. K.; Chen, H.; Ding, X.; Dipasquale, A. G.; Dominguez, S. L.; Dotson, J.; Drummond, J.; Flagella, M.; Flynn, S.; Fuji, R.; Gill, A.; Gunzner-Toste, J.; Harris, S. F.; Heffron, T. P.; Kleinheinz, T.; Lee, D. W.; Le Pichon, C. E.; Lyssikatos, J. P.; Medhurst, A. D.; Moffat, J. G.; Mukund, S.; Nash, K.; Scearce-Levie, K.; Sheng, Z.; Shore, D. G.; Tran, T.; Trivedi, N.; Wang, S.; Zhang, S.; Zhang, X.; Zhao, G.; Zhu, H.; Sweeney, Z. K. *J. Med. Chem.* **2012**, *55*, 9416–9433.

[8]   Henderson, J. L.; Kormos, B. L.; Hayward, M. M.; Coffman, K. J.; Jasti, J.; Kurumbail, R. G.; Wager, T. T.; Verhoest, P. R.; Noell, G. S.; Chen, Y.; Needle, E.; Berger, Z.; Steyn, S. J.; Houle, C.; Hirst, W. D.; Galatsis, P. *J. Med. Chem.* **2015**, *58*, 419–432.

[9]   Scott, J. D.; DeMong, D. E.; Greshock, T. J.; Basu, K.; Dai, X.; Harris, J.; Hruza, A.; Li, S. W.; Lin, S.-I.; Liu, H.; Macala, M. K.; Hu, Z.; Mei, H.; Zhang, H.; Walsh, P.; Poirier, M.; Shi, Z.; Xiao, L.; Agnihotri, G.; Baptista, M. A. S.; Columbus, J.; Fell, M. J.; Hyde, L. A.; Kuvelkar, R.; Lin, Y.; Mirescu, C.; Morrow, J. A.; Yin, Z.; Zhang, X.; Zhou, X.; Chang, R. K.; Embrey, M. W.; Sanders, J. M.; Tiscia, H. E.; Drolet, R. E.; Kern, J. T.; Sur, S. M.; Renger, J. J.; Bilodeau, M. T.; Kennedy, M. E.; Parker, E. M.; Stamford, A. W.; Nargund, R. P.; McCauley, J. A.; Miller, M. W. *J. Med. Chem.* **2017**, *60*, 2983–2992.

[10]   Ou, S. H. I. *Drug Des. Devel. Ther.* **2011**, *5*, 471–485.

[11]   Glide, Schrödinger, LLC, New York, NY. Release 2016-U4.

[12]   Wager, T. T.; Hou, X.; Verhoest, P. R.; Villalobos, A. *ACS Chem. Neurosci.* **2010**, *1*, 435–449.

[13]   Edwards, M. P.; Price, D. A. *Role of Physicochemical Properties and Ligand Lipophilicity Efficiency in Addressing Drug Safety Risks*; Elsevier Inc., **2010**; Vol. 45.

[14]   Graves, L. M.; Litchfield, D. W. *Chem. Biol.* **2011**, *18*, 683–684.

Supplementary Material

Description of the protocol for the LRRK2 G2019S and WT Lanthascreen assay, Kinativ[TM] screening data for compound **45** and synthesis of compound **45**.